Nanoimprinted Patterned Pillar Substrates for Surface-Enhanced Raman Scattering Applications

Juhong Chen,[†] Yinyong Li,[‡] Kang Huang,[†] Panxue Wang,[†] Lili He,[†] Kenneth R. Carter,[‡] and Sam R. Nugen*,[†]

[†]Department of Food Science, University of Massachusetts, 102 Holdsworth Way, Amherst, Massachusetts 01003, United States

[‡]Department of Polymer Science and Engineering, University of Massachusetts, 120 Governors Drive, Amherst, Massachusetts 01003, United States

S *Supporting Information*

ABSTRACT: A pragmatic method to deposit silver nanoparticles on polydopamine-coated nanoimprinted pillars for use as surface-enhanced Raman scattering (SERS) substrates was developed. Pillar arrays consisting of poly(methyl methacrylate) (PMMA) that ranged in diameter from 300 to 500 nm were fabricated using nanoimprint lithography. The arrays had periodicities from 0.6 to 4.0 μm. A polydopamine layer was coated on the pillars in order to facilitate the reduction of silver ions to create silver nucleation sites during the electroless deposition of sliver nanoparticles. The size and density of silver nanoparticles were controlled by adjusting the growth time for the optimization of the SERS performance. The size of the surface-adhered nanoparticles ranged between 75 and 175 nm, and the average particle density was ∼30 particles per μm^2. These functionalized arrays had a high sensitivity and excellent signal reproducibility for the SERS-based detection of 4-methoxybenzoic acid. The substrates were also able to allow the SERS-based differentiation of three types of bacteriophages (λ, T3, and T7).

KEYWORDS: surface-enhanced Raman scattering, silver nanoparticle, pillar array, nanoimprint lithography, bacteriophage discrimination
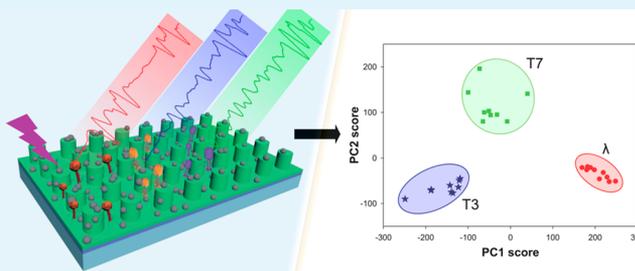
INTRODUCTION

Nanostructures of gold and silver can generate localized surface plasmon resonances and greatly enhance an electromagnetic field, providing excellent surface-enhanced Raman scattering (SERS) capacity.[1−3] Due to its high sensitivity for the detection of chemical and biological agents,[4−6] SERS has gained increased attention as a powerful analytical technique for the detection of a single molecule.[2,7] The strong signal enhancement is attributed to the formation of hotspots at nanogaps (<10 nm) or interstitial junctions between metallic nanostructures.[8] To date, most research has focused on the fabrication of high surface area SERS substrates with an increased density of hotspots in order to improve SERS sensitivity.[9−11] For example, using sputtered silver to abridge a gold pillar tip spacing[12] and silver nanoislands on glass nanopillars were demonstrated to significantly enhance a SERS signal.[13] Additionally, electrospun titanium dioxide nanofibers coated with silver nanoparticles (AgNPs) have also been shown to be sensitive SERS substrates.[14,15] Although these above-mentioned SERS substrates are highly sensitive, are reproducible, and have site-independent hotspots, their fabrication is complicated and not cost-effective. Therefore, there is a compelling need to rapidly fabricate an inexpensive, highly sensitive, and reproducible SERS substrate as a chemical and biochemical sensing platform.

Since the initial report of mussel-inspired surface chemistry to prepare multifunctional coatings,[16] poly(dopamine) (PDA) coatings have become a powerful tool for the development of functional patterns of cells, proteins, and metal nanoparticles.[17−20] PDA has the ability to be coated on almost all types of organic and inorganic substrates, and it is biocompatible with biomolecules.[21] The catechol, amine, and imide groups on the surface of PDA can reduce silver ions and bind AgNPs, creating a functional layer for SERS, antibacterial, and catalytic applications.[21−26] The mild reducing conditions for the conversion of noble metal ions into metallic nanoparticles allow for the uniform deposition of AgNPs on the PDA surface, and these surfaces yield reproducible Raman spectra. The size and morphology of AgNPs can be controlled to optimize the SERS performance. Therefore, PDA has shown potential for the fabrication of reproducible and sensitive SERS substrates.

Herein, we demonstrate a simple, rapid, and effective method to uniformly deposit AgNPs on pillar substrates for SERS analysis. To accomplish this, poly(methyl methacrylate) pillar

arrays on silicon substrates were prepared using thermal nanoimprint lithography (NIL).[27,28] Compared to a planar surface, pillars, which are high surface area structured substrates, offer a higher density of hotspots and a greater number of binding sites for molecules.[29] The fabrication of the pillar structures can readily be scaled up on flexible substrates using a continuous roll-to-roll NIL system, providing an opportunity for low-cost and high-volume manufacturing.[30] After preparation of the pillar arrays, PDA was self-assembled on the pillars and facilitated the reduction of silver ions into AgNPs as seeds for growth of AgNPs. The AgNP growth time was optimized to control their size and density, creating a large number of hotspots to generate strong SERS signals. The AgNP-decorated pillar SERS substrates were employed in the label-free detection and discrimination of bacteriophages, demonstrating a promising SERS application for virus detection.

EXPERIMENTAL SECTION

Chemicals and Materials. Silver nitrate, hydrogen peroxide (30%), and anisole were purchased from Acros Organics (Morris Plains, NJ). Tris base, sulfuric acid, and ethylenediaminetetraacetic acid (EDTA) were purchased from Fisher Scientific (Fair Lawn, NJ). Poly(methyl methacrylate) (PMMA, M_w = 100 000), 4-methoxybenzoic acid (4-MBA), dopamine hydrochloride, and catechol were purchased from Sigma-Aldrich (Saint Louis, MO). A thermally cross-linkable polydimethylsiloxane formulation, Sylgard 184 elastomer mixture kit, was purchased from Fisher Scientific (Fair Lawn, NJ), and the cured form of this resin will be referred to in this manuscript simply as PDMS. Silicon wafers (5 in., n-type, As-doped, [100]) were purchased from El-Cat, Inc. All chemicals were reagent-grade and used as received.

Instrumentation. Thermal nanoimprint lithography was performed on a Nanonex NX-2000 Nanoimprintor (Nanonex, Princeton, NJ). The surface morphologies of fabricated pillar substrates were characterized using a FEI scanning electron microscope (SEM, Hillsboro, OR) with current of 13 pA and voltage of 1 kV. The surface-enhanced Raman spectroscopic (SERS) studies were performed using a Thermo Scientific DXR Raman Spectro-microscope (Madison, WI) with a 780 nm laser source. The measurements were performed under the following conditions: 10× objective, 3.1 μm spot diameter, 5 mW laser power, 2 s, and 25 μm slit width for 4-MBA; and 50× objective, 1 μm spot diameter, 1 mW laser power, 2 s, and 50 μm slit width for bacteriophages. In this study, a minimum of 10 spots on each sample were randomly measured with a range of 400–2000 cm^{-1}. The Raman spectra were analyzed using Thermo Scientific TQ Analyst software (version 8.0). The average SERS intensities were calculated from at least three independent samples.

Fabrication of PMMA Pillars. PDMS daughter molds were replicated from silicon masters with varying pillar array patterns (diameter of 300–500 nm, period of 0.6–4 μm, and height of 500 nm). Briefly, a PDMS elastomer mixture (10:1 weight ratio of Sylgard 184 silicone elastomer base and curing agent) was poured on top of the silicon master mold and cured at 60 °C for 8 h. After curing, the PDMS mold was peeled from the silicon master.

The PMMA pillars were prepared using thermal nanoimprint lithography (NIL). The silicon wafer substrates were sonicated in ethanol and acetone for 5 min, immersed into piranha solution (mixture of sulfuric acid and hydrogen peroxide (30%) at 3:1 in volume) for 2 h at 70 °C, washed with deionized (DI) water, and dried under nitrogen gas. A solution of PMMA in anisole (8.0 wt %) was spin-coated on the cleaned wafers at 3000 rpm for 60 s and baked at 100 °C for 30 min. The thickness of the PMMA layer was ~260 nm. The PDMS molds were imprinted into the PMMA layer using the nanoimprintor under a pressure of 2069 kPa at 120 °C for 2 min.

Depositing of Silver Nanoparticle Seeds on Polydopamine Coating. A thin polydopamine layer was self-polymerized on the PMMA pillars using previously described methods.[16,21] Accordingly,

the nanoimprinted pillars were immersed into a dopamine solution (0.5 mg mL^{-1} in 10 mM Tris buffer, pH 8.5) with gentle agitation at room temperature for 2 h. The pillars were rinsed with DI water and dried under nitrogen gas. A layer of AgNPs seeds was formed on the polydopamine-coated pillars by submerging the substrates into silver nitrate solution (50 mM) with gentle agitation at room temperature. After 3 h, the substrates were washed with DI water and dried with nitrogen gas.

Growth of Silver Nanoparticles. The silver-plating solution was prepared according to the reported method with slight modifications.[23] Silver nitrate (40 mg) was dissolved in 10 mL of DI water. EDTA solution (0.5 M, 10 mL, pH 7.0) was deposited dropwise into the silver nitrate solution until it became clear. The pillar substrates were then immersed into the silver-plating solution, and 20 μL of a catechol solution (50 mg mL^{-1}) was added immediately. After allowing time for the reduction of silver ions (10–120 min), the wafers were washed with DI water and dried under nitrogen gas.

Discrimination of Bacteriophages. Bacteriophages (phages) are viruses that can infect and replicate within specific bacteria resulting in bacteria lysis. The seed phages were added to 10 mL of *E. coli* BL21 cultures (OD$_{600}$ = ~0.6) and incubated until the solutions became clear. The solution was then centrifuged at 8 000 × g for 10 min to remove bacterial debris. The supernatant was centrifuged and washed two additional times at 35 000 × g for 2 h to purify the phages. The bacteriophage titer was determined using standard plaque assay.[31−33] For this study, three phages (λ, T3, and T7) were characterized on the SERS substrate. The SERS substrate (**pillar-7**) was then incubated in the purified phage solutions at a concentration of 10^6 PFU mL^{-1} for 1 h, which allowed the phage to bind to AgNPs prior to recording the SERS spectra.

RESULTS AND DISCUSSION

The growth of AgNPs on pillars is illustrated in Figure 1. The procedure started with using NIL to create PMMA pillars on
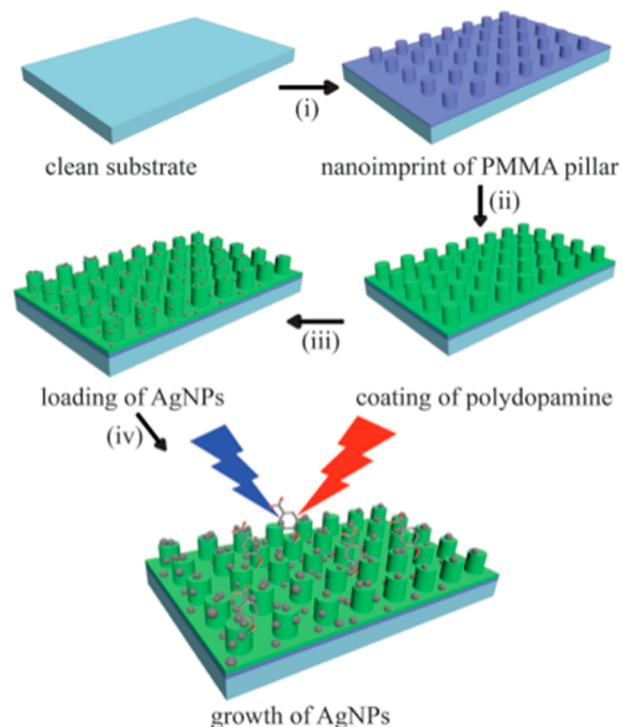

Figure 1. Schematic illustration of steps taken to fabricate SERS substrates consisting of silver nanoparticle decorated on pillars: (i) nanoimprinting of PMMA pillars; (ii) coating of poly(dopamine) layer; (iii) deposition of silver nanoparticle seeds; and (iv) growth of silver nanoparticles.
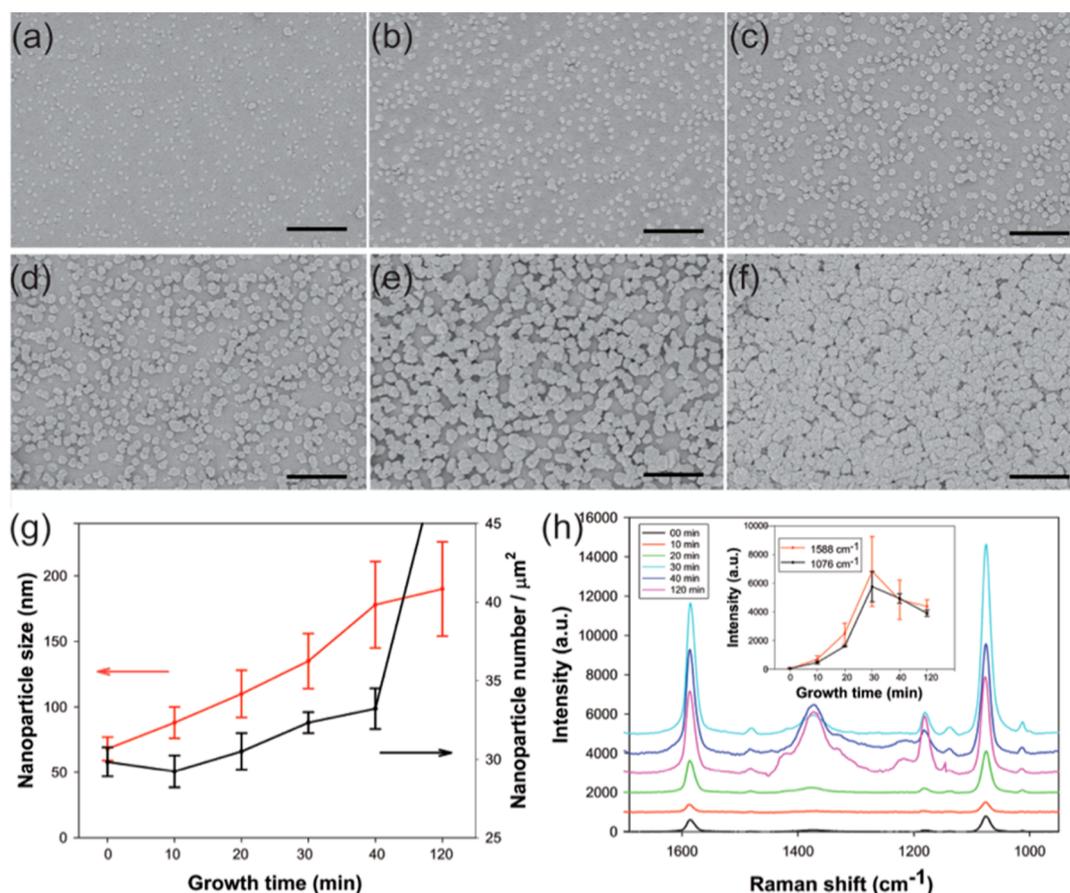
Figure 2. SEM images of AgNPs grown from planar surfaces at different growth times: (a) AgNP seeds, (b) 10 min, (c) 20 min, (d) 30 min, (e) 40 min, and (f) 120 min. (The scale bar represents 1 μm.) (g) Plots of the size and density of AgNPs on the planar surfaces as a function of growth time. (h) SERS spectra of 4-MBA at a concentration of 10^{-4} M on the planar surfaces that were prepared using different growth times (inset shows the relationship between growth time and Raman intensity at 1588 and 1076 cm^{-1}).

clean silicon wafer using a PDMS mold. These pillars were treated with dopamine in an alkaline pH environment, resulting in dopamine polymerization on the surface of the PMMA pillars.[16] By varying the reaction time, the thickness of self-polymerized polydopamine was controlled.[21,34] The multifunctional groups presented by the polydopamine-coated surface can be utilized to reduce silver ions into a seed layer of AgNPs.[35,36] The AgNPs were ripened by placing the seeded substrates in a silver-plating solution in the presence of a reducing agent. The final size and density of AgNPs on the pillar substrates were optimized by controlling the growth time as confirmed by SERS performance.

To investigate the effect of growth time on the size and density of AgNPs, planar PMMA-coated surfaces were used as a model. These flat substrates provide samples that are relatively easy to characterize by SEM and present no additional topological constraints. After coating with polydopamine, the substrates were incubated in a silver nitrate solution for 3 h. This resulted in the formation of a sparsely populated layer of AgNP seeds (Figure 2a) with a diameter and density of 68 ± 9 nm and 30 ± 1 per μm^2, respectively. Because of the small size and low density of AgNPs, the substrate gave a weak SERS response. To increase the density size of the AgNPs, the seeded substrates were placed into a silver-plating solution for varying times (10, 20, 30, 40, and 120 min). The representative SEM images of the samples following particle growth are shown in Figure 2b–f. The size and density of the AgNPs at different

growth times were calculated based on 100 AgNPs selected randomly on the SEM images. Additionally, the size distributions of AgNPs at each growth time were analyzed to determine the uniformity of the surface (Figure S1). As shown in Figure 2g, the diameter of AgNPs increased with additional growth time. Meanwhile, the density of AgNPs was initially constant but increased following 20 min of incubation. Small AgNP nuclei appeared at 30 munites, resulting in the higher density of AgNPs. After plating for 2 h, a bright brown AgNP film with larger AgNPs can be observed, and it became impractical to count the number of AgNPs.

To investigate the effect of growth time on the SERS performance, 4-MBA was selected for SERS detection. The different substrates were incubated in 4-MBA ethanol solutions at a concentration of 10^{-4} M for 2 h and then washed with ethanol to remove any unbound 4-MBA. After drying at room temperature, the SERS spectra were taken for the substrates prepared at different growth times (Figure 2h). The distinct Raman peaks of 4-MBA located at 1588, 1178, 1130, and 1076 cm^{-1} were consistent with previous reports.[37,38] The weak Raman peaks at 1178 and 1130 cm^{-1} were attributed to δ(C–H) deformation modes. Other vibrational modes including ν(C–C) ring stretching (1588 cm^{-1}) and ν(C–C) ring breathing (1076 cm^{-1}) were also observed.[38,39] The peak intensities at 1588 and 1076 cm^{-1} were plotted as a function of growth time (Figure 2h, inset). Substrates grown for 30 min gave the highest Raman intensities at peaks of the referenced
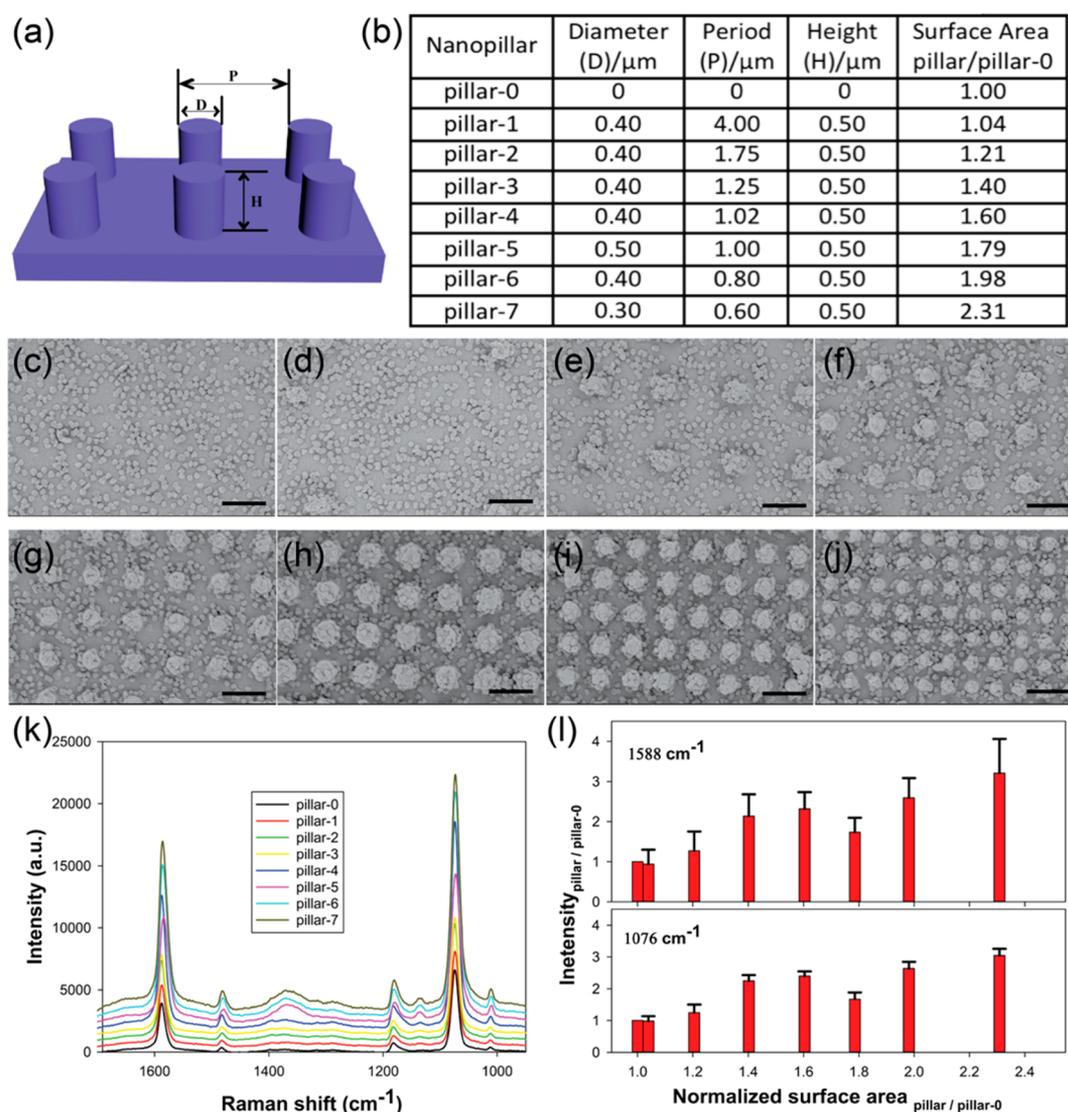
Figure 3. (a) Schematic illustration of surface pillars (*D*, diameter; *P*, period; and *H*, height). (b) List of different pillar samples. SEM images of AgNPs after growth for 30 min on (c) planar surface, (d) pillar-1, (e) pillar-2, (f) pillar-3, (g) pillar-4, (h) pillar-5, (i) pillar-6, and (j) pillar-7. (The scale bar represents 1 μm.) (k) SERS spectra of 4-MBA (10^{-4} M) absorbed on eight kinds of pillars, and (l) plot of normalized intensity versus normalized surface area of different pillars at (top) 1588 cm^{-1} and (bottom) 1076 cm^{-1}.

peaks, which suggested that optimal SERS performance is related to an appropriate size and density of AgNPs on the substrate. The growth in silver-plating solution for 30 min resulted in an AgNP with size of 135 ± 21 nm and density of 32 ± 1 per μm^2.

Next, pillar textured substrates were examined first using the substrate labeled **pillar-2** (pillar diameter, *D* = 0.40 μm; periodicity, *P* = 1.25 μm; and height, *H* = 0.50 μm). The PDA coating and subsequent AgNP growth was accomplished as described earlier for the planar substrates. The data suggested that a growth time of 30 min resulted in the optimal SERS signal (Figure S2). Hence, a growth time of 30 min was selected for further fabrication of AgNP-decorated pillars for subsequent SERS measurements.

The AgNP-coated pillar substrates listed in Figure 3b were fabricated using the same fabrication procedures and AgNP growth time as the planar substrates. The SEM images of these substrates are shown in Figure 3c−j. SEM analysis revealed that the size and density of AgNPs on these pillar surfaces were comparable to those formed on planar surfaces. The SERS

spectra of these pillar substrates are shown in Figure 3k. The peaks at 1588, 1178, 1130, and 1076 cm^{-1} were also observed, which was consistent with the observations made using the planar substrates. The Raman intensities of the pillar substrates were normalized using the planar surface substrate as control at 1588 and 1076 cm^{-1}. To further determine the effect of pillar diameter and period on Raman intensity, the normalized SERS intensities at 1588 and 1076 cm^{-1} were plotted with respect to normalized surface area. As shown in Figure 3l, the SERS intensity increased with the increase of normalized surface area. After comparing these pillar substrates, sample **pillar-7** showed the best SERS performance and was selected as the substrate for further experiments. This conclusion can also be obtained from the relationship between the normalized SERS intensity and the normalized surface area at 1076 cm^{-1}.

It is clear that the strong enhancement came from the hotspots at nanogaps or interstitial junctions between the AgNPs. The Raman enhancement factor (EF) of our fabricated **pillar-7** substrate was calculated using the reported method (see details in Supporting Information).[40] Although the Raman
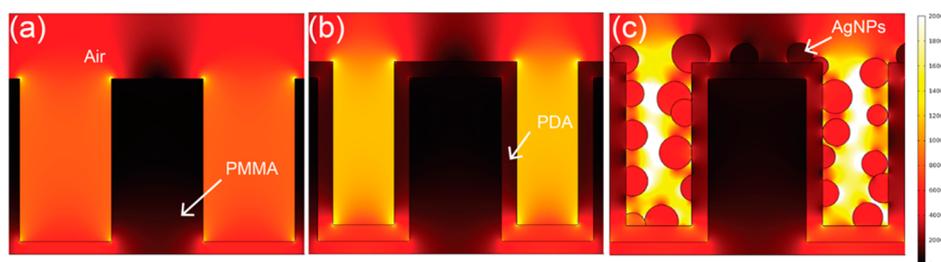
Figure 4. Electromagnetic near-field enhancement simulating results using FEA analysis at the excitation laser wavelength (780 nm): (a) nanoimprinted pillar, (b) PDA-coated pillar, and (c) AgNP-deposited pillar.
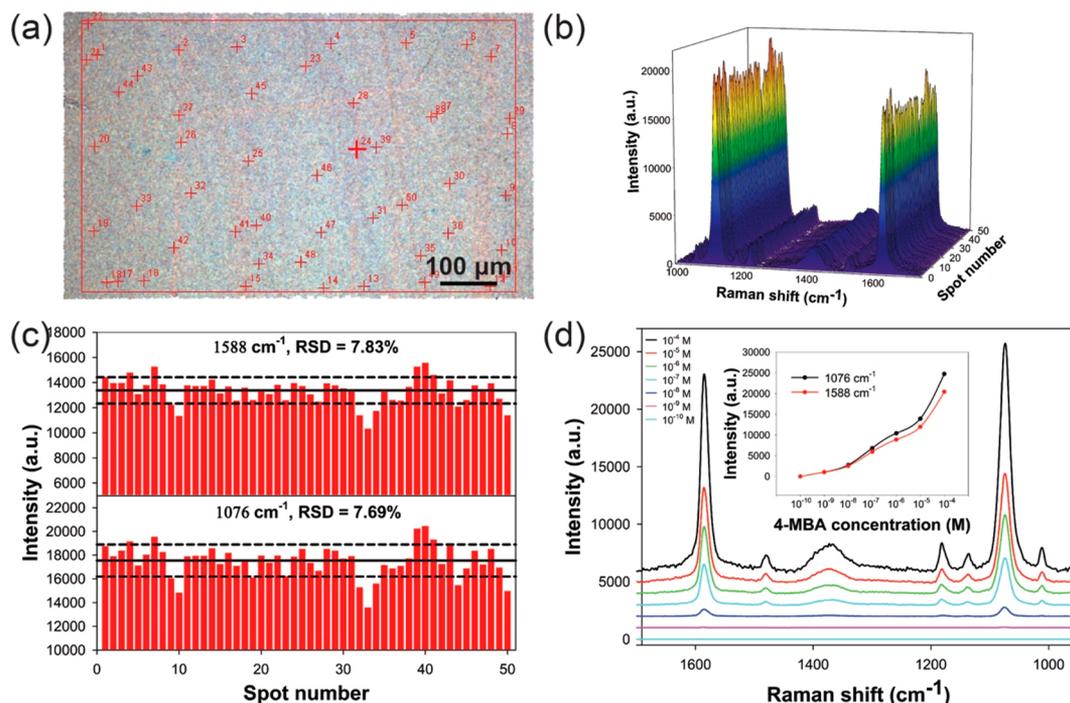

Figure 5. (a) Mapping image of 50 spots randomly selected on sample **pillar-7**. (b) Collective SERS spectra of 4-MBA (10^{-4} M) for all 50 spots. (c) SERS intensity distribution of the peaks at 1588 and 1076 cm^{-1} (the solid line indicates the average of intensity, and the dashed line represents ± standard deviation intensity variation). (d) SERS spectra of 4-MBA at varying concentrations from 10^{-4} to 10^{-10} M (the inset is the relationship between Raman intensity at 1588 and 1076 cm^{-1} and the concentration of 4-MBA).

EF (1.4×10^5) of **pillar-7** substrate was smaller than high-active SERS substrates, our approach to fabricate this SERS substrate was rapid, simple, and effective. Furthermore, the Raman enhancement of our **pillar-7** was simulated using finite element analysis (FEA; Figure 4). As shown in Figure 4c, strong electric field spots were obtained, indicating the increase of hotspots.

It has been reported that the uniform distribution and deposition of AgNPs on pillar substrates contributes to good reproducibility of SERS spectra.[21,40,41] To evaluate the reproducibility of **pillar-7**, the pillar substrate was incubated in a 4-MBA ethanol solution (10^{-4} M) for 2 h. Fifty spots were randomly selected from a large area with a dimension of 800 μm in length and 500 μm in width (Figure 5a). The SERS spectra from 50 randomly selected spots were recorded (Figure 5a, b). To quantify and clarify the reproducibility of our substrates, the relative standard deviations (RSDs) of Raman intensities at 1588 and 1076 cm^{-1} peaks were calculated to be 7.83% and 7.69%, respectively (Figure 5c). The RSD values at both measurement points were smaller than 8.00%, revealing a very good uniformity and reproducibility across the whole pillar substrate. On the basis of the reported studies, these SERS

substrates were stable at ambient conditions.[42] The SERS spectra of 4-MBA at a range of concentrations from 10^{-4} M to 10^{-10} M were recorded. As shown in the inset of Figure 5d, this pillar substrate can be applied to detect 4-MBA with a concentration as low as 10^{-9} M (Figure S3).

A bacteriophage (also called phage) is a virus that infects and replicates within a host bacterial cell and can eventually kill the bacteria.[43,44] Because of the infection, phages have been used to control and test foodborne bacterial pathogens.[44−46] The discrimination and detection of several pathogens using SERS have previously been reported,[47−49] and the high reproducibility of the pillar substrates allowed them to be used in this complicated sensing application. In this study, we examined three types of phages with different sizes and surface compositions, which can infect and lead to the lysis of *Escherichia coli*. Phage λ has an icosahedral head of 50−60 nm in diameter and a long noncontractile tail of 150 nm.[50] Phage T3 and phage T7 have similar morphologies, a short noncontractile tail virus with 55 nm head in diameter and 28.5 nm tail.[51,52]
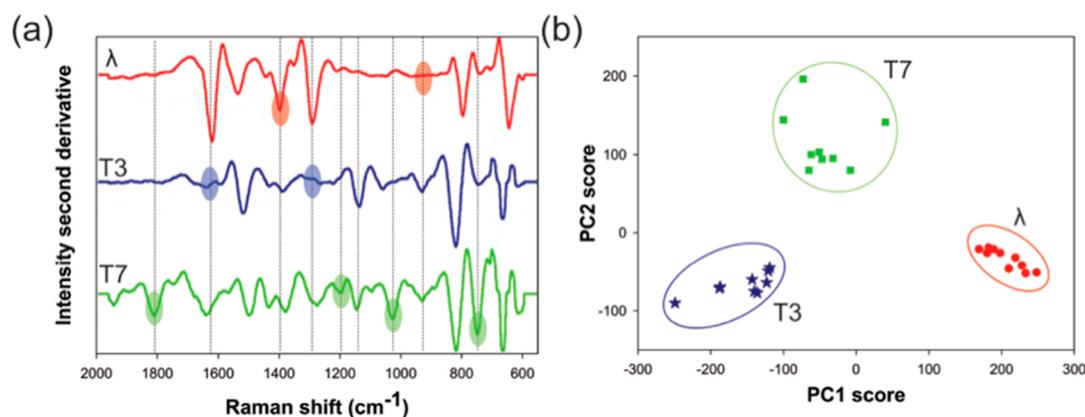
Figure 6. (a) SERS spectra (after secondary derivative transformation) of three bacteriophages at a concentration of 10^{-6} PFU mL^{-1} recorded on sample **pillar-7**. (b) Principle components analysis (PCA) plot of PC1 vs PC2 computed from the SERS spectra of three bacteriophages: phage λ, phage T3, and phage T7.

Compared to bacterial cells (size = 2−5 μm), phages with 50−200 nm length were able to better locate among AgNPs to ensure the strong SERS intensity. A solution of each phage (10^6 PFU mL^{-1}) was measured on the **pillar-7** substrate. The second derivative spectra of the three phages are shown in Figure 6a, serving as fingerprints for differentiation and detection of phages. The phage SERS spectra shared some common spectral features; however, noticeable differences did appear in the spectra, which are marked using dotted line and colored circles in Figure 6a. The principal components analysis (PCA) can reduce a multidimensional data set and retain its most dominant features. The variance between different classes and within a class can also be obtained from the PCA plot. Here, the PCA was used to investigate the differences of these phage spectra.[53] The PCA result shows the clusterings of different sample data can be clearly separated, indicating that the SERS method can effectively discriminate these different phages (Figure 6b). To our knowledge, this is the first report to distinguish bacteriophages using SERS spectra as fingerprints.[54] These AgNP-decorated pillar substrates have great potential to be applied in a SERS-based detection in food safety, clinic diagnostics, and environmental monitoring.

CONCLUSIONS

We have demonstrated a rapid, simple, and effective approach to fabricate substrates containing pillars decorated with silver nanoparticles (AgNPs) that show excellent SERS performance. The AgNPs were uniformly dispersed, and both the size and density of the nanoparticles was tunable, creating numerous hotspots. These substrates provided excellent signal reproducibility (RSD < 8.00%) and a limit of detection for 4-MBA as low as 10^{-9} M. Moreover, the pillar-structured label-free SERS substrate was successfully applied for the detection and discrimination of three types of bacteriophages. This improved approach could open a new avenue to prepare a low-cost, fast, and simple platform for efficient SERS-based detection and differentiation of chemical and biological agents.

ASSOCIATED CONTENT

Ⓢ **Supporting Information**

The Supporting Information is available free of charge on the ACS Publications website at DOI: 10.1021/acsami.5b07879.

Size-distribution analysis of silver nanoparticle after different growth times, SEM images of silver nano-

particles on **pillar-2** substrate, SERS spectra of 4-MBA on **pillar-2** substrate, relationship between growth time and SERS intensity, and calculation of Raman enhancement factor (PDF)

AUTHOR INFORMATION

Corresponding Author

*Tel.: +1-413-545-1025; Fax: +1-413-545-1262; E-mail: snugen@umass.edu.

Notes

The authors declare no competing financial interest.

REFERENCES

(1) Liang, H.; Li, Z.; Wang, W.; Wu, Y.; Xu, H. Highly Surface-Roughened "Flower-Like" Silver Nanoparticles for Extremely Sensitive Substrates of Surface-Enhanced Raman Scattering. *Adv. Mater.* **2009**, *21* (45), 4614−4618.

(2) Kneipp, K.; Wang, Y.; Kneipp, H.; Perelman, L. T.; Itzkan, I.; Dasari, R. R.; Feld, M. S. Single Molecule Detection Using Surface-Enhanced Raman Scattering (SERS). *Phys. Rev. Lett.* **1997**, *78* (9), 1667.

(3) Gandra, N.; Singamaneni, S. Bilayered Raman-Intense Gold Nanostructures with Hidden Tags (BRIGHTS) for High-Resolution Bioimaging. *Adv. Mater.* **2013**, *25* (7), 1022−1027.

(4) Guerrini, L.; Graham, D. Molecularly-Mediated Assemblies of Plasmonic Nanoparticles for Surface-Enhanced Raman Spectroscopy Applications. *Chem. Soc. Rev.* **2012**, *41* (21), 7085−7107.

(5) Zavaleta, C. L.; Smith, B. R.; Walton, I.; Doering, W.; Davis, G.; Shojaei, B.; Natan, M. J.; Gambhir, S. S. Multiplexed Imaging of Surface Enhanced Raman Scattering Nanotags in Living Mice Using Noninvasive Raman Spectroscopy. *Proc. Natl. Acad. Sci. U. S. A.* **2009**, *106* (32), 13511−13516.

(6) Cao, Y. C.; Jin, R.; Mirkin, C. A. Nanoparticles with Raman Spectroscopic Fingerprints for DNA and RNA Detection. *Science* **2002**, *297* (5586), 1536−1540.

(7) Kodiyath, R.; Wang, J.; Combs, Z. A.; Chang, S.; Gupta, M. K.; Anderson, K. D.; Brown, R. J.; Tsukruk, V. V. SERS Effects in Silver-Decorated Cylindrical Nanopores. *Small* **2011**, *7* (24), 3452−3457.

(8) Ward, D. R.; Grady, N. K.; Levin, C. S.; Halas, N. J.; Wu, Y.; Nordlander, P.; Natelson, D. Electromigrated Nanoscale Gaps for Surface-Enhanced Raman Spectroscopy. *Nano Lett.* **2007**, *7* (5), 1396−1400.

(9) Fan, M.; Andrade, G. F.; Brolo, A. G. A Review on the Fabrication of Substrates for Surface Enhanced Raman Spectroscopy and Their Applications in Analytical Chemistry. *Anal. Chim. Acta* **2011**, *693* (1), 7−25.

(10) Lin, X.-M.; Cui, Y.; Xu, Y.-H.; Ren, B.; Tian, Z.-Q. Surface-Enhanced Raman Spectroscopy: Substrate-Related Issues. *Anal. Bioanal. Chem.* **2009**, *394* (7), 1729−1745.

(11) Kumar, G. V. P. Plasmonic Nano-Architectures for Surface Enhanced Raman Scattering: A Review. *J. Nanophotonics* **2012**, *6* (1), 064503.

(12) Huang, Z. L.; Meng, G. W.; Huang, Q.; Yang, Y. J.; Zhu, C. H.; Tang, C. L. Improved SERS Performance from Au Nanopillar Arrays by Abridging the Pillar Tip Spacing by Ag Sputtering. *Adv. Mater.* **2010**, *22* (37), 4136−4139.

(13) Oh, Y. J.; Jeong, K. H. Glass Nanopillar Arrays with Nanogap-Rich Silver Nanoislands for Highly Intense Surface Enhanced Raman Scattering. *Adv. Mater.* **2012**, *24* (17), 2234−2237.

(14) Zhao, Y.; Sun, L.; Xi, M.; Feng, Q.; Jiang, C.; Fong, H. Electrospun TiO$_2$ Nanofelt Surface-Decorated with Ag Nanoparticles as Sensitive and UV-Cleanable Substrate for Surface Enhanced Raman Scattering. *ACS Appl. Mater. Interfaces* **2014**, *6* (8), 5759−5767.

(15) Zhang, L.; Gong, X.; Bao, Y.; Zhao, Y.; Xi, M.; Jiang, C.; Fong, H. Electrospun Nanofibrous Membranes Surface-Decorated with Silver Nanoparticles as Flexible and Active/Sensitive Substrates for Surface-Enhanced Raman Scattering. *Langmuir* **2012**, *28* (40), 14433−14440.

(16) Lee, H.; Dellatore, S. M.; Miller, W. M.; Messersmith, P. B. Mussel-Inspired Surface Chemistry for Multifunctional Coatings. *Science* **2007**, *318* (5849), 426−430.

(17) Chien, H.-W.; Kuo, W.-H.; Wang, M.-J.; Tsai, S.-W.; Tsai, W.-B. Tunable Micropatterned Substrates Based on Poly(Dopamine) Deposition Via Microcontact Printing. *Langmuir* **2012**, *28* (13), 5775−5782.

(18) Sun, K.; Xie, Y.; Ye, D.; Zhao, Y.; Cui, Y.; Long, F.; Zhang, W.; Jiang, X. Mussel-Inspired Anchoring for Patterning Cells Using Polydopamine. *Langmuir* **2012**, *28* (4), 2131−2136.

(19) Chien, H.-W.; Tsai, W.-B. Fabrication of Tunable Micropatterned Substrates for Cell Patterning Via Microcontact Printing of Polydopamine with Poly(Ethylene Imine)-Grafted Copolymers. *Acta Biomater.* **2012**, *8* (10), 3678−3686.

(20) Rodriguez-Emmenegger, C.; Preuss, C. M.; Yameen, B.; Pop-Georgievski, O.; Bachmann, M.; Mueller, J. O.; Bruns, M.; Goldmann, A. S.; Bastmeyer, M.; Barner-Kowollik, C. Controlled Cell Adhesion on Poly(Dopamine) Interfaces Photopatterned with Non-Fouling Brushes. *Adv. Mater.* **2013**, *25* (42), 6123−6127.

(21) Akin, M. S.; Yilmaz, M.; Babur, E.; Ozdemir, B.; Erdogan, H.; Tamer, U.; Demirel, G. Large Area Uniform Deposition of Silver Nanoparticles through Bio-Inspired Polydopamine Coating on Silicon Nanowire Arrays for Practical SERS Applications. *J. Mater. Chem. B* **2014**, *2* (30), 4894.

(22) Sureshkumar, M.; Lee, P.-N.; Lee, C.-K. Stepwise Assembly of Multimetallic Nanoparticles Via Self-Polymerized Polydopamine. *J. Mater. Chem.* **2011**, *21* (33), 12316.

(23) Long, Y.; Wu, J.; Wang, H.; Zhang, X.; Zhao, N.; Xu, J. Rapid Sintering of Silver Nanoparticles in an Electrolyte Solution at Room Temperature and Its Application to Fabricate Conductive Silver Films Using Polydopamine as Adhesive Layers. *J. Mater. Chem.* **2011**, *21* (13), 4875.

(24) Dong, H.; Zhao, Y.; Tang, Y.; Burkert, S. C.; Star, A. Oxidative Unzipping of Stacked Nitrogen-Doped Carbon Nanotube Cups. *ACS Appl. Mater. Interfaces* **2015**, *7* (20), 10734−10741.

(25) Murali, S.; Xu, T.; Marshall, B. D.; Kayatin, M. J.; Pizarro, K.; Radhakrishnan, V. K.; Nepal, D.; Davis, V. A. Lyotropic Liquid Crystalline Self-Assembly in Dispersions of Silver Nanowires and Nanoparticles. *Langmuir* **2010**, *26* (13), 11176−11183.

(26) Wang, S.; Wan, Y.; Liu, Y. Effects of Nanopillar Array Diameter and Spacing on Cancer Cell Capture and Cell Behaviors. *Nanoscale* **2014**, *6* (21), 12482−12489.

(27) Maruf, S. H.; Wang, L.; Greenberg, A. R.; Pellegrino, J.; Ding, Y. Use of Nanoimprinted Surface Patterns to Mitigate Colloidal Deposition on Ultrafiltration Membranes. *J. Membr. Sci.* **2013**, *428* (0), 598−607.

(28) Chen, J.; Zhou, Y.; Wang, D.; He, F.; Rotello, V. M.; Carter, K. R.; Watkins, J. J.; Nugen, S. R. UV-Nanoimprint Lithography as a Tool to Develop Flexible Microfluidic Devices for Electrochemical Detection. *Lab Chip* **2015**, *15* (14), 3086−3094.

(29) Kodiyath, R.; Papadopoulos, T. A.; Wang, J.; Combs, Z. A.; Li, H.; Brown, R. J.; Brédas, J.-L.; Tsukruk, V. V. Silver-Decorated Cylindrical Nanopores: Combining the Third Dimension with Chemical Enhancement for Efficient Trace Chemical Detection with SERS. *J. Phys. Chem. C* **2012**, *116* (26), 13917−13927.

(30) John, J.; Tang, Y.; Rothstein, J. P.; Watkins, J. J.; Carter, K. R. Large-Area, Continuous Roll-to-Roll Nanoimprinting with PFPE Composite Molds. *Nanotechnology* **2013**, *24* (50), 505307.

(31) Lillehaug, D. An Improved Plaque Assay for Poor Plaque-Producing Temperate Lactococcal Bacteriophages. *J. Appl. Microbiol.* **1997**, *83* (1), 85−90.

(32) Tawil, N.; Sacher, E.; Mandeville, R.; Meunier, M. Bacteriophages: Biosensing Tools for Multi-Drug Resistant Pathogens. *Analyst* **2014**, *139* (6), 1224−1236.

(33) Liebana, S.; Spricigo, D. A.; Cortes, M. P.; Barbe, J.; Llagostera, M.; Alegret, S.; Pividori, M. I. Phagomagnetic Separation and Electrochemical Magneto-Genosensing of Pathogenic Bacteria. *Anal. Chem.* **2013**, *85* (6), 3079−3086.

(34) Bernsmann, F.; Ball, V.; Addiego, F.; Ponche, A.; Michel, M.; Gracio, J. J. d. A.; Toniazzo, V.; Ruch, D. Dopamine-Melanin Film Deposition Depends on the Used Oxidant and Buffer Solution. *Langmuir* **2011**, *27* (6), 2819−2825.

(35) Sureshkumar, M.; Siswanto, D. Y.; Lee, C.-K. Magnetic Antimicrobial Nanocomposite Based on Bacterial Cellulose and Silver Nanoparticles. *J. Mater. Chem.* **2010**, *20* (33), 6948−6955.

(36) Lee, Y.; Park, T. G. Facile Fabrication of Branched Gold Nanoparticles by Reductive Hydroxyphenol Derivatives. *Langmuir* **2011**, *27* (6), 2965−2971.

(37) Hunyadi, S. E.; Murphy, C. J. Bimetallic Silver−Gold Nanowires: Fabrication and Use in Surface-Enhanced Raman Scattering. *J. Mater. Chem.* **2006**, *16* (40), 3929−3935.

(38) Yan, J.; Han, X.; He, J.; Kang, L.; Zhang, B.; Du, Y.; Zhao, H.; Dong, C.; Wang, H. L.; Xu, P. Highly Sensitive Surface-Enhanced Raman Spectroscopy (SERS) Platforms Based on Silver Nanostructures Fabricated on Polyaniline Membrane Surfaces. *ACS Appl. Mater. Interfaces* **2012**, *4* (5), 2752−2756.

(39) Amarjargal, A.; Tijing, L. D.; Shon, H. K.; Park, C.-H.; Kim, C. S. Facile in Situ Growth of Highly Monodispersed Ag Nanoparticles on Electrospun Pu Nanofiber Membranes: Flexible and High Efficiency Substrates for Surface Enhanced Raman Scattering. *Appl. Surf. Sci.* **2014**, *308*, 396−401.

(40) He, L. F.; Huang, J. A.; Xu, T. T.; Chen, L. M.; Zhang, K.; Han, S. T.; He, Y.; Lee, S. T. Silver Nanosheet-Coated Inverse Opal Film as a Highly Active and Uniform SERS Substrate. *J. Mater. Chem.* **2012**, *22* (4), 1370−1374.

(41) Shao, F.; Lu, Z. C.; Liu, C.; Han, H. Y.; Chen, K.; Li, W. T.; He, Q. G.; Peng, H.; Chen, J. N. Hierarchical Nanogaps within Bioscaffold Arrays as a High-Performance SERS Substrate for Animal Virus Biosensing. *ACS Appl. Mater. Interfaces* **2014**, *6* (9), 6281−6289.

(42) Wang, P.; Zhou, Y.; Wen, Y.; Wang, F.; Yang, H. In Situ Polydopamine-Assisted Deposition of Silver Nanoparticles on a Two Dimensional Support as an Inexpensive and Highly Efficient SERS Substrate. *RSC Adv.* **2015**, *5* (46), 36368−36373.

(43) Chen, J.; Duncan, B.; Wang, Z.; Wang, L.-S.; Rotello, V. M.; Nugen, S. R. Bacteriophage-Based Nanoprobes for Rapid Bacteria Separation. *Nanoscale* **2015**, DOI: 10.1039/C5NR03779D.

(44) Chen, J.; Alcaine, S. D.; Jiang, Z.; Rotello, V. M.; Nugen, S. R. Detection of *Escherichia Coli* in Drinking Water Using T7

Bacteriophage-Conjugated Magnetic Probe. *Anal. Chem.* **2015**, *87* (17), 8977−8984.

(45) Abuladze, T.; Li, M.; Menetrez, M. Y.; Dean, T.; Senecal, A.; Sulakvelidze, A. Bacteriophages Reduce Experimental Contamination of Hard Surfaces, Tomato, Spinach, Broccoli, and Ground Beef by *Escherichia Coli* O157:H7. *Appl. Environ. Microbiol.* **2008**, *74* (20), 6230−6238.

(46) Goodridge, L. D.; Bisha, B. Phage-Based Biocontrol Strategies to Reduce Foodborne Pathogens in Foods. *Bacteriophage* **2011**, *1* (3), 130−137.

(47) Jarvis, R. M.; Goodacre, R. Discrimination of Bacteria Using Surface-Enhanced Raman Spectroscopy. *Anal. Chem.* **2004**, *76* (1), 40−47.

(48) Patel, I.; Premasiri, W.; Moir, D.; Ziegler, L. Barcoding Bacterial Cells: A SERS-Based Methodology for Pathogen Identification. *J. Raman Spectrosc.* **2008**, *39* (11), 1660−1672.

(49) Premasiri, W.; Moir, D.; Klempner, M.; Krieger, N.; Jones, G.; Ziegler, L. Characterization of the Surface Enhanced Raman Scattering (SERS) of Bacteria. *J. Phys. Chem. B* **2005**, *109* (1), 312−320.

(50) Hendrix, R. W.; Duda, R. L. Bacteriophage Lambda Papa: Not the Mother of All Lambda Phages. *Science* **1992**, *258* (5085), 1145−1148.

(51) Fraikin, J.-L.; Teesalu, T.; McKenney, C. M.; Ruoslahti, E.; Cleland, A. N. A High-Throughput Label-Free Nanoparticle Analyser. *Nat. Nanotechnol.* **2011**, *6* (5), 308−313.

(52) Hancock, R. E.; Reeves, P. Bacteriophage Resistance in *Escherichia Coli* K-12: General Pattern of Resistance. *J. Bacteriol.* **1975**, *121* (3), 983−993.

(53) He, L.; Deen, B. D.; Pagel, A. H.; Diez-Gonzalez, F.; Labuza, T. P. Concentration, Detection and Discrimination of *Bacillus Anthracis* Spores in Orange Juice Using Aptamer Based Surface Enhanced Raman Spectroscopy. *Analyst* **2013**, *138* (6), 1657−1659.

(54) Goeller, L. J.; Riley, M. R. Discrimination of Bacteria and Bacteriophages by Raman Spectroscopy and Surface-Enhanced Raman Spectroscopy. *Appl. Spectrosc.* **2007**, *61* (7), 679−685.